Mineralogy of an ancient lacustrine mudstone succession from the Murray formation, Gale crater, Mars

E B Rampe, D W Ming, D F Blake, T F Bristow, S J Chipera, J P Grotzinger, R V Morris, S M Morrison, D T Vaniman, A S Yen, et al.

▶ **To cite this version:**

E B Rampe, D W Ming, D F Blake, T F Bristow, S J Chipera, et al.. Mineralogy of an ancient lacustrine mudstone succession from the Murray formation, Gale crater, Mars. Earth and Planetary Science Letters, 2017, 471, pp.172 - 185. 10.1016/j.epsl.2017.04.021 . insu-03211833

HAL Id: insu-03211833
https://insu.hal.science/insu-03211833

Submitted on 29 Apr 2021

HAL is a multi-disciplinary open access archive for the deposit and dissemination of scientific research documents, whether they are published or not. The documents may come from teaching and research institutions in France or abroad, or from public or private research centers.

L'archive ouverte pluridisciplinaire **HAL**, est destinée au dépôt et à la diffusion de documents scientifiques de niveau recherche, publiés ou non, émanant des établissements d'enseignement et de recherche français ou étrangers, des laboratoires publics ou privés.

Earth and Planetary Science Letters 471 (2017) 172–185

Contents lists available at ScienceDirect

Earth and Planetary Science Letters

www.elsevier.com/locate/epsl

Mineralogy of an ancient lacustrine mudstone succession from the Murray formation, Gale crater, Mars

E.B. Rampe [a,*], D.W. Ming [a], D.F. Blake [b], T.F. Bristow [b], S.J. Chipera [c], J.P. Grotzinger [d], R.V. Morris [a], S.M. Morrison [e,f], D.T. Vaniman [g], A.S. Yen [h], C.N. Achilles [e], P.I. Craig [i], D.J. Des Marais [b], R.T. Downs [e], J.D. Farmer [j], K.V. Fendrich [e], R. Gellert [k], R.M. Hazen [f], L.C. Kah [l], J.M. Morookian [h], T.S. Peretyazhko [m], P. Sarrazin [n], A.H. Treiman [h], J.A. Berger [o], J. Eigenbrode [p], A.G. Fairén [q,r], O. Forni [s], S. Gupta [t], J.A. Hurowitz [u], N.L. Lanza [v], M.E. Schmidt [w], K. Siebach [d], B. Sutter [m], L.M. Thompson [x]

[a] *Astromaterials Research and Exploration Science Division, NASA Johnson Space Center, Houston, TX 77058, USA*
[b] *NASA Ames Research Center, Moffett Field, CA 94035, USA*
[c] *Chesapeake Energy, Oklahoma City, OK 73154, USA*
[d] *Division of Geologic and Planetary Sciences, California Institute of Technology, Pasadena, CA 91125, USA*
[e] *Department of Geosciences, University of Arizona, Tucson, AZ 85721, USA*
[f] *Geophysical Laboratory, Carnegie Institution of Washington, Broad Branch Rd NW, Washington, DC 20015, USA*
[g] *Planetary Science Institute, Tucson, AZ 85719, USA*
[h] *Jet Propulsion Laboratory, California Institute of Technology, Pasadena, CA 91109, USA*
[i] *Lunar and Planetary Institute, Houston, TX 77058, USA*
[j] *School of Earth and Space Exploration, Arizona State University, Tempe, AZ 85287, USA*
[k] *Department of Physics, University of Guelph, Guelph, ON N1G 2W1, Canada*
[l] *Department of Earth and Planetary Science, University of Tennessee, Knoxville, TN 37996, USA*
[m] *Jacobs – JETS Contract, Houston, TX 77058, USA*
[n] *SETI Institute, Mountain View, CA 94043, USA*
[o] *Department of Earth Sciences, University of Western Ontario, London, ON N6A 5B7, Canada*
[p] *NASA Goddard Space Flight Center, Greenbelt, MD 20771, USA*
[q] *Centro de Astrobiología, CSIC-INTA, 28850 Madrid, Spain*
[r] *Department of Astronomy, Cornell University, Ithaca, NY 14853, USA*
[s] *Institut de Recherche en Astrophysique et Planétologie, CNRS, UMR 5277, Toulouse, France*
[t] *Department of Earth Sciences and Engineering, Imperial College London, London SW7 2AZ, UK*
[u] *Department of Geosciences, Stony Brook University, Stony Brook, NY 11794, USA*
[v] *Los Alamos National Laboratory, Los Alamos, NM 87545, USA*
[w] *Department of Earth Sciences, Brock University, St. Catharines, ON L25 3A1, Canada*
[x] *Planetary and Space Science Centre, University of New Brunswick, Fredericton, NB E3B 5A3, Canada*

ARTICLE INFO

Article history:
Received 3 August 2016
Received in revised form 3 April 2017
Accepted 12 April 2017
Available online 12 May 2017
Editor: C. Sotin

Keywords:
Mars
Gale crater
X-ray diffraction
diagenesis
acid-sulfate alteration

ABSTRACT

The Mars Science Laboratory *Curiosity* rover has been traversing strata at the base of Aeolis Mons (informally known as Mount Sharp) since September 2014. The Murray formation makes up the lowest exposed strata of the Mount Sharp group and is composed primarily of finely laminated lacustrine mudstone intercalated with rare crossbedded sandstone that is prodeltaic or fluvial in origin. We report on the first three drilled samples from the Murray formation, measured in the Pahrump Hills section. Rietveld refinements and FULLPAT full pattern fitting analyses of X-ray diffraction patterns measured by the MSL CheMin instrument provide mineral abundances, refined unit-cell parameters for major phases giving crystal chemistry, and abundances of X-ray amorphous materials. Our results from the samples measured at the Pahrump Hills and previously published results on the Buckskin sample measured from the Marias Pass section stratigraphically above Pahrump Hills show stratigraphic variations in the mineralogy; phyllosilicates, hematite, jarosite, and pyroxene are most abundant at the base of the Pahrump Hills, and crystalline and amorphous silica and magnetite become prevalent higher in the succession. Some trace element abundances measured by APXS also show stratigraphic trends; Zn and Ni are highly enriched with respect to average Mars crust at the base of the Pahrump Hills (by 7.7 and 3.7 times, respectively), and gradually decrease in abundance in stratigraphically higher regions

* Corresponding author.
E-mail address: elizabeth.b.rampe@nasa.gov (E.B. Rampe).

http://dx.doi.org/10.1016/j.epsl.2017.04.021
0012-821X/Published by Elsevier B.V. This is an open access article under the CC BY-NC-ND license (http://creativecommons.org/licenses/by-nc-nd/4.0/).

near Marias Pass, where they are depleted with respect to average Mars crust (by more than an order of magnitude in some targets). The Mn stratigraphic trend is analogous to Zn and Ni, however, Mn abundances are close to those of average Mars crust at the base of Pahrump Hills, rather than being enriched, and Mn becomes increasingly depleted moving upsection. Minerals at the base of the Pahrump Hills, in particular jarosite and hematite, as well as enrichments in Zn, Ni, and Mn, are products of acid-sulfate alteration on Earth. We hypothesize that multiple influxes of mildly to moderately acidic pore fluids resulted in diagenesis of the Murray formation and the observed mineralogical and geochemical variations. The preservation of some minerals that are highly susceptible to dissolution at low pH (e.g., mafic minerals and fluorapatite) suggests that acidic events were not long-lived and that fluids may not have been extremely acidic (pH > 2). Alternatively, the observed mineralogical variations within the succession may be explained by deposition in lake waters with variable Eh and/or pH, where the lowermost sediments were deposited in an oxidizing, perhaps acidic lake setting, and sediments deposited in the upper Pahrump Hills and Marias Pass were deposited lake waters with lower Eh and higher pH.

Published by Elsevier B.V. This is an open access article under the CC BY-NC-ND license (http://creativecommons.org/licenses/by-nc-nd/4.0/).

1. Introduction

The Mars Science Laboratory (MSL) *Curiosity* rover landed on the plains of Gale crater (Aeolis Palus) to the north of Aeolis Mons (informally known as Mount Sharp) in August 2012 to investigate a site presumed to have a variety of ancient aqueous environments and to assess the habitability of these environments (Grotzinger et al., 2012). Visible/short-wave infrared spectra from the Compact Reconnaissance Imaging Spectrometer for Mars (CRISM) on the Mars Reconnaissance Orbiter show stratigraphic trends in mineralogy in the lower sedimentary layers of Mount Sharp; the lowermost layers contain phyllosilicate, sulfate, and/or iron oxide minerals, with spectral evidence for phyllosilicate minerals decreasing up section (Milliken et al., 2010; Fraeman et al., 2013). Stratigraphic changes in mineralogy suggest that the rocks in lower Mount Sharp record an environmental transition from one in which phyllosilicate minerals formed to one in which sulfate minerals formed (Milliken et al., 2010). By studying the mineralogy and geochemistry of this sedimentary succession in situ with *Curiosity*, we can identify changes in environment and sediment sources on a much finer scale.

Bedrock exposed on the plains north of Mount Sharp belongs to strata of the Bradbury group and includes mudstone, sandstone, and conglomerate sequences deposited in fluvial-lacustrine environments (Grotzinger et al., 2014, 2015; Vasavada et al., 2014). The mudstone analyzed at Yellowknife Bay was interpreted as an ancient habitable lacustrine environment based on its mineralogical and geochemical composition (e.g., Grotzinger et al., 2014; McLennan et al., 2014; Ming et al., 2014; Vaniman et al., 2014), where circumneutral fluids with low ionic strength appear to be associated with the in-situ dissolution of olivine and precipitation of ferrian saponite and magnetite (Bristow et al., 2015). *Curiosity* reached the base of Mount Sharp in September 2014 in a region called the Pahrump Hills. Rocks of the Pahrump Hills make up the lowermost portion of the Murray formation and are dominated by finely horizontally laminated mudstone with minor intercalated cross-bedded sandstone, suggesting deposition from lacustrine to fluvial-deltaic environments (Grotzinger et al., 2015). The Murray formation is mapped as time-equivalent to coarser-grained strata of the Bradbury group, with fluvial-deltaic facies passing laterally into and interfingering with lacustrine facies.

The Murray formation was studied in detail at Pahrump Hills and at Marias Pass, 6 m stratigraphically above the top of the exposed section studied at the Pahrump Hills (Fig. 1). Detailed investigations in these locations included imaging by Mastcam and the Mars Hand Lens Imager (MAHLI), geochemical measurements by the Alpha Particle X-ray Spectrometer (APXS) and the Chemistry and Camera (ChemCam), and delivery of drilled rock powders to the instruments inside the body of the rover, the Chemistry and Mineralogy (CheMin) and Sample Analysis at Mars (SAM) instruments. Mineralogical results from CheMin for the Marias Pass drill sample are reported by Morris et al. (2016). Here, we report mineralogical results from CheMin of the samples collected from the Pahrump Hills section, including mineral abundances, refined unit-cell parameters, and derived crystal chemistry. We subsequently consider hypotheses about the depositional and diagenetic environments recorded in these rocks. Based on mineralogy, geochemistry, and diagenetic features, we propose a model of multiple acidic diagenetic fluid episodes. We also consider deposition in acid saline lakes as an explanation for the observed mineralogy.

2. Materials and methods

2.1. Samples

Four drill samples were acquired from the lower Murray formation by the MSL *Curiosity's* sample acquisition and handling system and delivered to CheMin for analysis (Figs. 1 and 2). Details of sample acquisition and processing by the Collection and Handling for In-situ Mars Rock Analysis (CHIMRA, Anderson et al., 2012) and analysis by the CheMin instrument are presented in the supplementary material. The first three samples were taken from the Pahrump Hills section of the Murray formation. The Confidence Hills (CH) and Mojave 2 (MJ) drill samples were acquired on sols 759 and 882, respectively, and lie near the base of the Pahrump Hills, with the MJ sample located 1.2 m stratigraphically above the CH drill site. The base of the Pahrump Hills records numerous features consistent with multiple diagenetic episodes, including centimeter-scale crystal clusters and dendrites enriched in Mg, Ni, and S, according to APXS measurements (Gellert et al., 2015a; Kah et al., 2015a; VanBommel et al., 2016); millimeter-scale lenticular crystal pseudomorphs (Kah et al., 2015b); and fractures containing one or two generations of mineral fill (including a late-diagenetic calcium-sulfate phase, Kah et al., 2015a, 2015b; Nachon et al., 2017). The Telegraph Peak (TP) sample was acquired on sol 908 at an elevation 7 m above the CH sample. Telegraph Peak lies just below a cross-stratified sandstone called Whale Rock, interpreted as a tongue of prodeltaic gulley or lowstand fluvial materials (Grotzinger et al., 2015). The Buckskin (BK) outcrop (sampled on sol 1060) is a ~2–3 m thick section of the Murray formation exposed in the Marias Pass region, 13 m upsection from CH (Morris, 2016).

2.2. Methods

All XRD data were first evaluated by comparisons and searches of the International Center for Diffraction Data (ICDD) Powder

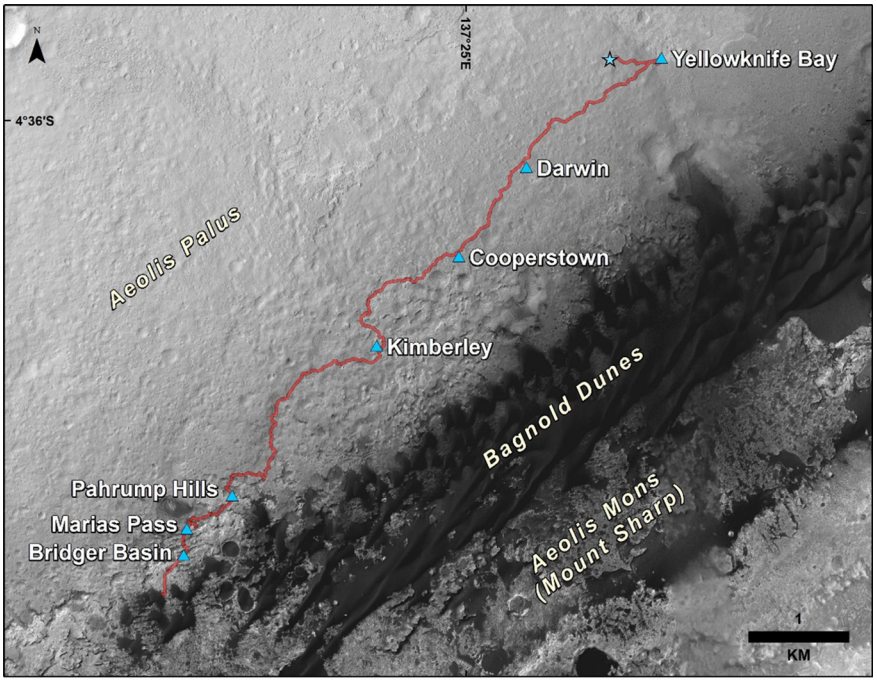

A

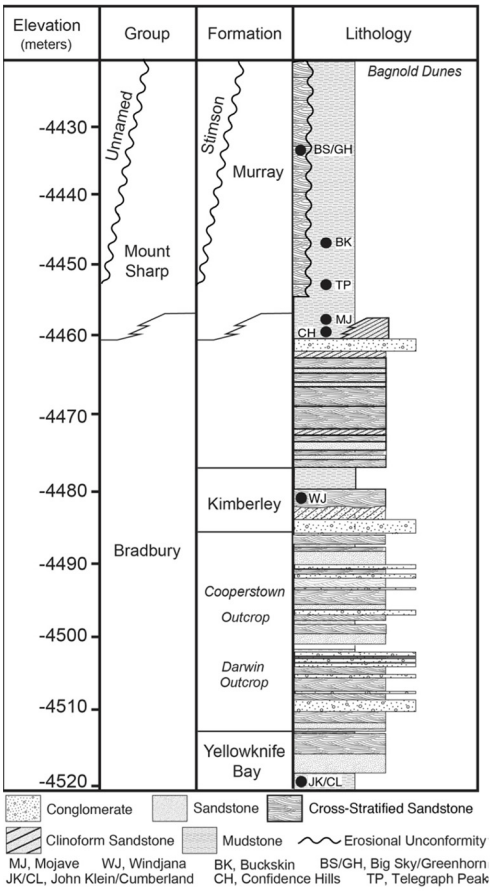

B

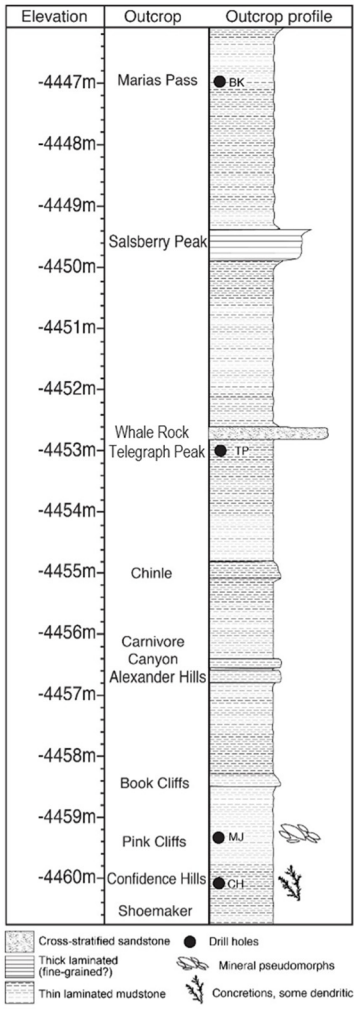

C

Fig. 1. A. *Curiosity's* traverse from landing through Sol 1185, showing locations of Pahrump Hills and Marias Pass. Image credit: NASA/JPL-Caltech/Univ. of Arizona. Map from http://mars.jpl.nasa.gov/msl/news/whatsnew/index.cformation?FuseAction=ShowNews& NewsID=1879. B. Stratigraphic column for the Bradbury and Mount Sharp groups, including all drill hole locations (Grotzinger et al., 2015). C. Stratigraphic column of the Murray formation, including the four sampling locations in this paper (Grotzinger et al., 2015).

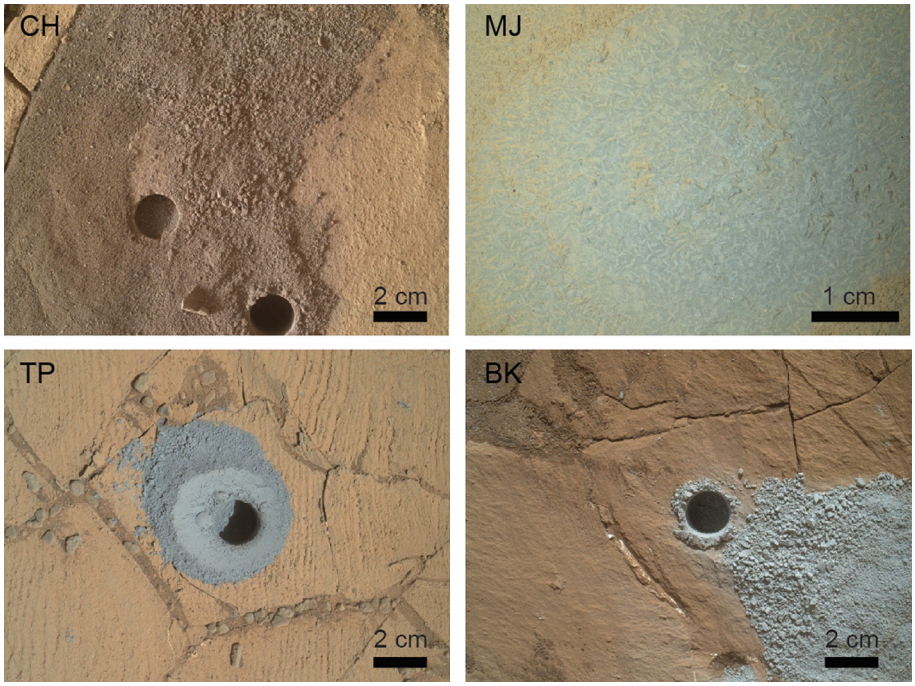

Fig. 2. Drill holes/targets for samples taken from the Murray formation and analyzed by CheMin. CH drill fines are redder than other samples, consistent with the greatest hematite abundance. MJ target shows lenticular white crystal forms in the mudstone. TP drill fines are gray, and the surrounding fine laminations are visible. BK drill fines are bright, consistent with abundant crystalline and amorphous SiO_2. Drill hole depths are ~6 cm, and samples delivered to CheMin are sourced from depths of ~5–6 cm. Images' credit: NASA/JPL-Caltech/MSSS.

Diffraction File using MDI Jade (Materials Data Incorporated, Livermore, CA) software packages. The data were analyzed further via Rietveld refinement methods, using Jade. The Rietveld method involves constructing a model consisting of the crystal structures of all component phases and minimizing the differences between the observed and simulated diffraction patterns by varying components of the model, including scale factors (related to phase abundance) and unit-cell parameters. This method thus provides information on all well-ordered crystalline phases, but is not directly applicable to disordered phases such as clay minerals or X-ray amorphous components.

Cell parameters for well-crystalline minerals present at >~5 wt.% abundance were refined using structure files from the American Mineralogist Crystal Structure Database. Abundances of phyllosilicate, poorly crystalline, and XRD-amorphous phases were estimated by the FULLPAT full pattern fitting method (Chipera and Bish, 2002) using laboratory patterns generated from CheMin IV, a laboratory prototype of the CheMin flight instrument.

Major, minor, and some trace element abundances were measured with the APXS located on the end of *Curiosity's* robotic arm (Campbell et al., 2012; Gellert et al., 2015b). The CheMin drill sample and the dump piles of post-sieved samples are nominally the same material (<150 μm), and, as such, these APXS analyses are the best comparison to CheMin results.

Chemical compositions of crystalline components comprising at least ~5 wt.% of the sample were estimated from unit-cell parameters calculated by Rietveld refinement. The calculations are insensitive, however, to trace element substitutions in the mineral structures. In order to limit artificial "assignments" of the trace elements to the amorphous material, we used compositions of naturally occurring minerals (from analyses of martian meteorites) to estimate the trace chemical compositions of the crystalline phases >5 wt.% (after Morris et al., 2016). The elemental composition of the X-ray amorphous±phyllosilicate components was estimated by mass balance calculations from the bulk APXS composition of the post-sieved dump pile, the inferred compositions of the crystalline phases, and the weight proportion of the X-ray amorphous and phyllosilicate components determined by FULLPAT (methods detailed by Vaniman et al., 2014; Morris et al., 2016).

3. Results

3.1. Confidence hills

The Confidence Hills (CH) sample provides our stratigraphically lowermost measurement of the Pahrump Hills section of the Murray formation. The major minerals present (>~5 wt.% of the crystalline phases) in this sample in decreasing order of abundance are: plagioclase, hematite, augite, pigeonite, sanidine, and magnetite (Fig. 3, Table 1). The broad diffraction peak near 10 Å indicates the presence of a poorly crystalline 2:1-layer type phyllosilicate. The identity of the phyllosilicate cannot be further constrained because of the absence of a distinct 02ℓ peak (e.g., Vaniman et al., 2014); the position of the 001 peak, however, is consistent with a collapsed smectite or illite (e.g., Moore and Reynolds, 1997). FULLPAT analysis of the CH pattern suggests this sample contains ~8 wt.% 2:1 layer type phyllosilicate. CH has the greatest abundances of mafic igneous minerals, phyllosilicate, and hematite of all samples presented in this manuscript.

Unit-cell parameters (Table 2) of plagioclase are consistent with andesine, $An_{42(10)}$ (Table 3, values in parentheses represent 2-sigma errors), and those of sanidine are in agreement with high sanidine, $Ab_{26(16)}Or_{74(16)}$, with complete Al–Si disorder. We derived a pigeonite composition of $En_{60(6)}Fs_{38(7)}Wo_{2(2)}$, however, the derived compositions and relative abundances of the pyroxenes have large uncertainties because of overlapping peaks and the low angular resolution of the CheMin instrument (0.3°2θ; Blake et al., 2012). The magnetite unit cell refined to an a unit-cell edge length of 8.365(6) Å, which indicates that magnetite is intermediate to stoichiometric magnetite and maghemite if we assume that Fe is the only cation in the mineral (e.g., Schwertmann and Cornell, 2000). The derived formula of magnetite is $Fe_{2.81(5)}\square_{0.19}O_4$

(where □ represents a vacancy) assuming it is cation deficient. Cation-deficient magnetite is an intermediate phase as magnetite oxidizes to maghemite (γ-Fe_2O_3) accompanied by loss of 11% Fe from the structure (Schwertmann and Cornell, 2000). Smaller *a*-cell lengths can also be achieved by substitution for Fe in the structure by other metals. Cation-substitutions are common in magnetite found in natural terrestrial settings and martian meteorites, and substitution primarily occurs on the octahedral site (e.g., Stout and Bayliss, 1980; Collyer, 1986). Substitutions that can create small *a*-cell lengths include Cr^{3+} and Al^{3+} for Fe^{3+} and Mg^{2+} and Ni^{2+} for Fe^{2+} (Figure S2).

Minor minerals identified from the CH pattern include orthopyroxene, jarosite, fluorapatite, forsterite, and quartz. We did not refine the unit-cell parameters for these phases because their peaks were not sharp, had low intensity, and often overlapped diffraction peaks from other, more abundant minerals. We are, however, confident in the presence of these phases. We also investigated the possible presence of other minerals which refined to abundances below the CheMin detection limit (~1 wt.%), including ilmenite, anhydrite, and anatase. These minerals did not fit discrete peaks, but including them in the Rietveld refinement improved the overall fit. As such, we cannot be certain of their presence and we do not include them in our reported mineral abundances.

The FULLPAT analysis gives 40 ± 15 wt.% X-ray amorphous materials, including truly amorphous materials and those with short-range atomic order. The amorphous component was modeled primarily as rhyolitic volcanic glass plus basaltic volcanic glass, with a small proportion of ferrihydrite. Note that this is a model, and that amorphous phases do not give definitive X-ray diffraction peaks, so that other amorphous materials absent from the FULLPAT library may also fit the measured data.

The poorly crystalline components (amorphous+phyllosilicate) in CH contain substantial iron and titanium (15.6 wt.% FeO_{total} and 2.3 wt.% TiO_2), are strongly enriched in volatiles (~11 wt.% $SO_3 + P_2O_5 + Cl$), and are slightly enriched in SiO_2 (52.6 wt.% SiO_2) compared to the bulk CH sample (Table S1). This calculated composition includes elemental abundances from crystalline phases that are below the CheMin detection limit. Cations that may be associated with the volatiles include Fe^{2+}, Fe^{3+}, Mg^{2+}, Al^{3+}, Na^+, Ca^{2+}, and K^+. The K_2O abundance in the amorphous+phyllosilicate component is low (0.3 wt.%, equivalent to ~3 wt.% illite), suggesting that the phyllosilicate in CH is likely not discrete illite or mica. High abundances of Fe and Mg (15.6 wt.% FeO_T and 5.5 wt.% MgO) are consistent with ferrian saponite, as reported for Yellowknife Bay (Vaniman et al., 2014; Treiman et al., 2014; Bristow et al., 2015).

3.2. Mojave 2

The MJ sample, from the Pahrump Hills section, was acquired ~1 m stratigraphically above CH. The major minerals (>~ 5 wt.% of the crystalline phases) in decreasing abundance are: plagioclase, pigeonite, hematite, magnetite, and jarosite (Fig. 3, Table 1). A weak, broad peak near 10 Å indicates the presence of a poorly crystalline phyllosilicate. The specific identity of the phyllosilicate in MJ cannot be determined with CheMin data alone, but the position of the 001 peak is consistent with a collapsed smectite or illite. FULLPAT analysis of the MJ pattern suggests this sample contains ~5 wt.% 2:1 layer type phyllosilicate. MJ has the highest abundance of jarosite with respect to all samples measured from the Murray formation and is the only one with no detectable sanidine.

The refined unit-cell parameters (Table 2) yield a composition of $An_{41(6)}$ for the plagioclase and $En_{61(9)}Fs_{37(11)}Wo_{2(4)}$ for the pigeonite. The magnetite unit cell refined to 8.357(4) Å, and the formula is $Fe_{2.77(7)}\square_{0.23}O_4$ assuming it only contains Fe. These compositions are within error of those determined for CH.

Minor phases identified from the MJ pattern include augite, fluorapatite, quartz, and forsterite. Unit-cell parameters were not refined for these phases. Other phases that improve the overall fit to the measured pattern are ilmenite, anatase, and anhydrite. These phases, however, do not fit discrete peaks, so we cannot conclude with certainty that they are present and we do not include them in the reported mineral abundances (Table 1).

Analysis by FULLPAT indicates that MJ contains ~41 ± 15 wt.% X-ray amorphous materials. The amorphous component was modeled primarily with rhyolitic and basaltic glasses with a small proportion of ferrihydrite. With this value, the calculated chemical composition of the poorly crystalline material has a negative CaO concentration. This impossible result can stem from (1) underestimating the abundance of X-ray amorphous materials and phyllosilicate or (2) overestimating the abundance of Ca-bearing minerals in the crystalline material. If abundances of X-ray amorphous materials and phyllosilicate are underestimated, then increasing their proportion from ~41% to ~53 wt.% brings the calculated CaO abundance in the poorly crystalline material to zero. This newly calculated composition for the poorly crystalline components (Table S2) is strongly enriched in volatiles (~11 wt.% $SO_3 + P_2O_5 + Cl$), iron, and titanium (12.7 wt.% FeO_{total} and 2.2 wt.% TiO_2). Similar to CH, the SiO_2 content of the poorly crystalline components (55.4 wt.% SiO_2) is slightly greater than the bulk rock (48.9 wt.% SiO_2). Cations that may be associated with the volatiles include Fe^{2+}, Fe^{3+}, Mg^{2+}, Al^{3+}, Na^+, and K^+. The K_2O abundance in the amorphous+phyllosilicate component is high enough to accommodate all phyllosilicate as illite, and there is abundant Fe and Mg (5.7 wt.% MgO), so we cannot constrain the identity of the phyllosilicate from these compositional calculations. If we assume that we are overestimating the abundance of Ca-bearing minerals, our identification of fluorapatite may not be correct. If we exclude fluorapatite from our calculations, the poorly crystalline material has a just positive CaO concentration. Including fluorapatite in our refinements, however, improves the fit. Furthermore, our detection of fluorapatite with CheMin in all samples from the Pahrump Hills is consistent with P_2O_5 abundances measured by APXS; P_2O_5 abundances calculated from CheMin-derived fluorapatite abundances are below the APXS measurements of P_2O_5, therefore requiring amorphous phosphate and/or the presence of a crystalline phosphate below the detection limits of CheMin. We hypothesize that FULLPAT models underestimated the abundance of X-ray amorphous materials in MJ; however, the updated value is within the error on the abundance derived from FULLPAT alone.

3.3. Telegraph peak

The TP drill sample was acquired ~7 m stratigraphically higher than CH. The major minerals (>~5 wt.% of crystalline phases) in TP are: plagioclase feldspar, magnetite, cristobalite, sanidine, pigeonite, and orthopyroxene (Fig. 3, Table 1). In contrast to CH and MJ, TP lacks a phyllosilicate signature. Of all samples measured from the Murray formation, TP contains the most magnetite and cristobalite.

The refined unit-cell parameters (Table 2) and crystal chemistry (Table 3) of plagioclase, sanidine, pigeonite, and magnetite in TP are similar to those for the other Pahrump Hills samples. The unit-cell parameters of plagioclase are consistent with $An_{37(7)}$. The unit-cell parameters of the alkali feldspar are consistent with high sanidine ($Ab_{39(25)}Or_{61(25)}$) and are within uncertainty of the sanidine composition refined in CH. The refined pigeonite unit-cell parameters suggest a composition of $En_{61(11)}Fs_{37(13)}Wo_{2(3)}$. The magnetite refined to a unit-cell *a*-value between those of stoi-

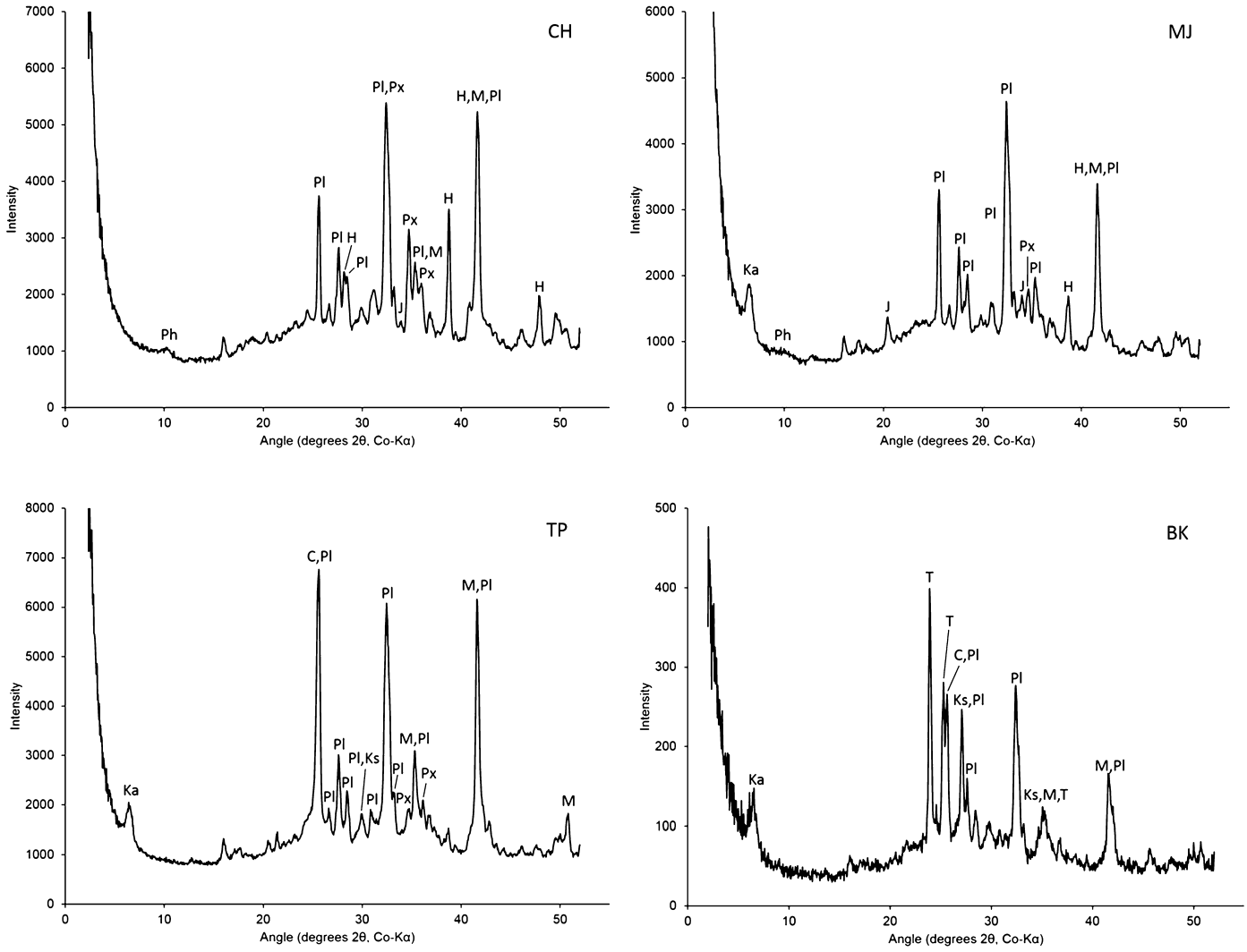

Fig. 3. CheMin 1-D X-ray diffraction patterns of samples taken from the Murray formation. Major peaks are labeled (A = anhydrite, C = cristobalite, H = hematite, J = jarosite, Ka = Kapton (part of the sample cell, not in the rock powders), Ks = K-feldspar, M = magnetite, Ph = phyllosilicate, Pl = plagioclase, Px = pyroxene, T = tridymite).

Table 1
Mineral and amorphous abundances in weight % of samples in the Murray formation measured by CheMin. 2-sigma errors are denoted in parentheses.

Mineral	Confidence Hills	Mojave 2	Telegraph Peak	Buckskin[a]
Plagioclase	20.4(2.3)	23.5(1.6)	27.1(2.8)	17.1(1.2)
Sanidine	5.0(0.7)	–	5.2(2.2)	3.4(0.7)
Forsterite	1.2(0.7)	0.2(0.8)	1.1(1.2)	–
Augite	6.4(2.2)	2.2(1.1)	–	–
Pigeonite	5.3(1.7)	4.6(0.7)	4.2(1.0)	–
Orthopyroxene	2.1(3.1)	–	3.4(2.6)	–
Magnetite	3.0(0.7)	3.0(0.6)	8.2(0.9)	2.8(0.3)
Hematite	6.8(1.5)	3.0(0.6)	1.1(0.5)	–
Quartz	0.7(0.5)	0.8(0.3)	0.9(0.4)	–
Cristobalite	–	–	7.3(1.7)	2.4(0.3)
Tridymite	–	–	–	13.6(0.8)
(H_3O^+, K^+, Na^+) Jarosite	1.1(0.7)	3.1(1.6)	1.5(1.8)	–
Anhydrite	–	–	–	0.7(0.2)
Fluorapatite	1.3(1.5)	1.8(1.0)	1.9(0.5)	–
Phyllosilicate[b]	7.6	4.7	–	–
Opal-CT	–	–	10.9	6.0
Amorphous	39.2 ± 15[b]	53[c]	27.2 ± 15[b]	54[c]

[a] Numbers reported by Morris et al. (2016).
[b] From FULLPAT analyses alone.
[c] From amorphous component calculations using CheMin and APXS results.

Table 2
Refined unit-cell parameters in angstroms for the major phases in the four samples measured from the Murray formation. 2-sigma errors are reported in parentheses, where the error is applied to the last decimal place(s).

Mineral	Parameter	Confidence Hills	Mojave 2	Telegraph Peak	Buckskin[a]
Plagioclase	a	8.166(15)	8.164(7)	8.157(3)	8.155(3)
	b	12.859(15)	12.859(5)	12.858(12)	12.862(4)
	c	7.111(7)	7.110(3)	7.111(2)	7.106(4)
	α	93.45(11)	93.50(8)	93.47(4)	93.32(2)
	β	116.31(8)	116.28(1)	116.28(2)	116.28(2)
	γ	90.15(9)	90.10(3)	90.08(2)	90.10(2)
Sanidine	a	8.582(10)	–	8.526(39)	8.54(2)
	b	13.009(26)	–	12.985(29)	13.01(2)
	c	7.158(18)	–	7.151(27)	7.15(2)
	β	115.95(26)	–	115.94(36)	115.8(1)
Pigeonite	a	9.651(32)	9.670(61)	9.670(71)	–
	b	8.920(41)	8.916(67)	8.926(84)	–
	c	5.210(31)	5.197(76)	5.194(71)	–
	β	108.57(17)	108.66(68)	108.62(42)	–
Magnetite	a	8.365(6)	8.357(4)	8.355(1)	8.359(1)
Hematite	a	5.029(1)	5.031(7)	–	–
	c	13.745(4)	13.791(9)	–	–
Cristobalite	a	–	–	4.981(24)	–
	c	–	–	6.979(81)	–
Tridymite	a	–	–	–	4.996(2)
	b	–	–	–	8.671(2)
	c	–	–	–	8.194(3)
	β	–	–	–	90.43(4)

[a] Numbers reported by Morris et al. (2016).

Table 3
Crystal chemistry of feldspars, pyroxene, and magnetite from their respective refined unit-cell parameters for the four samples measured from the Murray formation.

Mineral	Confidence Hills	Mojave 2	Telegraph Peak	Buckskin[a]
Plagioclase	$An_{42\pm10}Ab_{58\pm10}$	$An_{41\pm6}Ab_{59\pm6}$	$An_{37\pm7}Ab_{63\pm7}$	$An_{41\pm12}Ab_{59\pm12}$
Sanidine	$Ab_{26\pm16}Or_{74\pm16}$	–	$Ab_{39\pm25}Or_{61\pm25}$	$Ab_{32\pm16}Or_{68\pm16}$
Pigeonite	$En_{60(6)}Fs_{38(7)}Wo_{2(2)}$	$En_{61(9)}Fs_{37(11)}Wo_{2(4)}$	$En_{61(11)}Fs_{37(13)}Wo_{2(3)}$	–
Magnetite	$Fe_{2.81(5)}\square_{0.19}O_4$	$Fe_{2.77(7)}\square_{0.23}O_4$	$Fe_{2.76(7)}\square_{0.24}O_4$	$Fe_{2.78(10)}\square_{0.22}O_4$

[a] Crystal chemistry reported by Morris et al. (2016).

chiometric magnetite and maghemite (8.355(1) Å). The magnetite formula is $Fe_{2.76(7)}\square_{0.24}O_4$ assuming it is cation-deficient.

Minor phases identified through full pattern fitting of the TP data include fluorapatite, jarosite, hematite, quartz, and forsterite. We are confident in the presence of these minerals because their inclusion in refinements accounts for missing intensities of minor, but distinct peaks and improves the overall fit. Trace minerals that improve the fit to the measured data are anhydrite, bassanite, anatase, and brookite; however, these minerals improve the fit between peaks or on shoulders of peaks and do not fit discrete peaks, so we are not confident in their identification.

FULLPAT analysis revealed that TP contains 38 ± 15 wt.% XRD amorphous material. The X-ray amorphous component in TP was modeled primarily as rhyolitic and basaltic glasses, opal-CT, and a small proportion of ferrihydrite. The calculated amorphous composition (Table S3) has a volatile component (~8 wt.% $SO_3 + P_2O_5 +$ Cl), contains iron and titanium (19.6 wt.% FeO and 3.1 wt.% TiO_2), and is slightly enriched in SiO_2 (55.0 wt.% SiO_2) compared to the bulk sample (52.1 wt.% SiO_2). Cations that may be associated with the volatiles include Fe^{2+}, Fe^{3+}, Mg^{2+}, Al^{3+}, Na^+, Ca^{2+}, and K^+.

3.4. Buckskin

The mineral abundances, refined unit-cell parameters, and X-ray amorphous composition for the BK sample are described by Morris et al. (2016). Here, we briefly reiterate the main findings as background for the discussion of mineral trends in the Murray formation.

The BK drill sample was acquired at Marias Pass, ~13 m stratigraphically higher than CH. BK contains substantial amounts of plagioclase (andesine) and monoclinic tridymite, with lesser amounts of sanidine, magnetite, cristobalite, and anhydrite. BK does not contain phyllosilicates nor does it contain substantial mafic igneous minerals (magnetite is the only Fe-bearing mineral), and provides the first detection of tridymite on the surface of Mars. The refined magnetite has a unit-cell similar to that of the other Murray samples (8.359(1) Å), giving the formula $Fe_{2.78(10)}\square_{0.22}O_4$, and the refined sanidine composition is similar to those refined for CH and TP ($Ab_{32(16)}Or_{68(16)}$).

Buckskin is composed of ~60 wt.% X-ray amorphous materials, as determined by mass balance calculations using CheMin-derived crystalline component and chemistry measured by APXS. The amorphous component is enriched in SiO_2 (opal-A, silica glass, and/or opal-CT) and volatiles ($SO_3 + P_2O_5 +$ Cl) and contains minor iron and titanium (Table S4).

4. Discussion

4.1. Stratigraphic trends in mineralogy and chemistry

Depositional and diagenetic environments on modern and ancient Earth are characterized by detailed mineralogical, geochemical, and petrographic analyses and from thorough field campaigns. We recognize that we cannot fully capture the potential mineralogical heterogeneities of these deposits with *Curiosity*. Bowen et al. (2012), for example, have documented lateral mineralogical variations at the scales of thin section to outcrop, resulting from changes in water chemistry and sediment composition. Doing field work with a rover on Mars limits our ability to investigate lateral variations so that we can only have data from a 1-dimensional time series. Although we have not investigated lateral variability and we lack petrographic information about the samples measured from Gale crater to discriminate between the

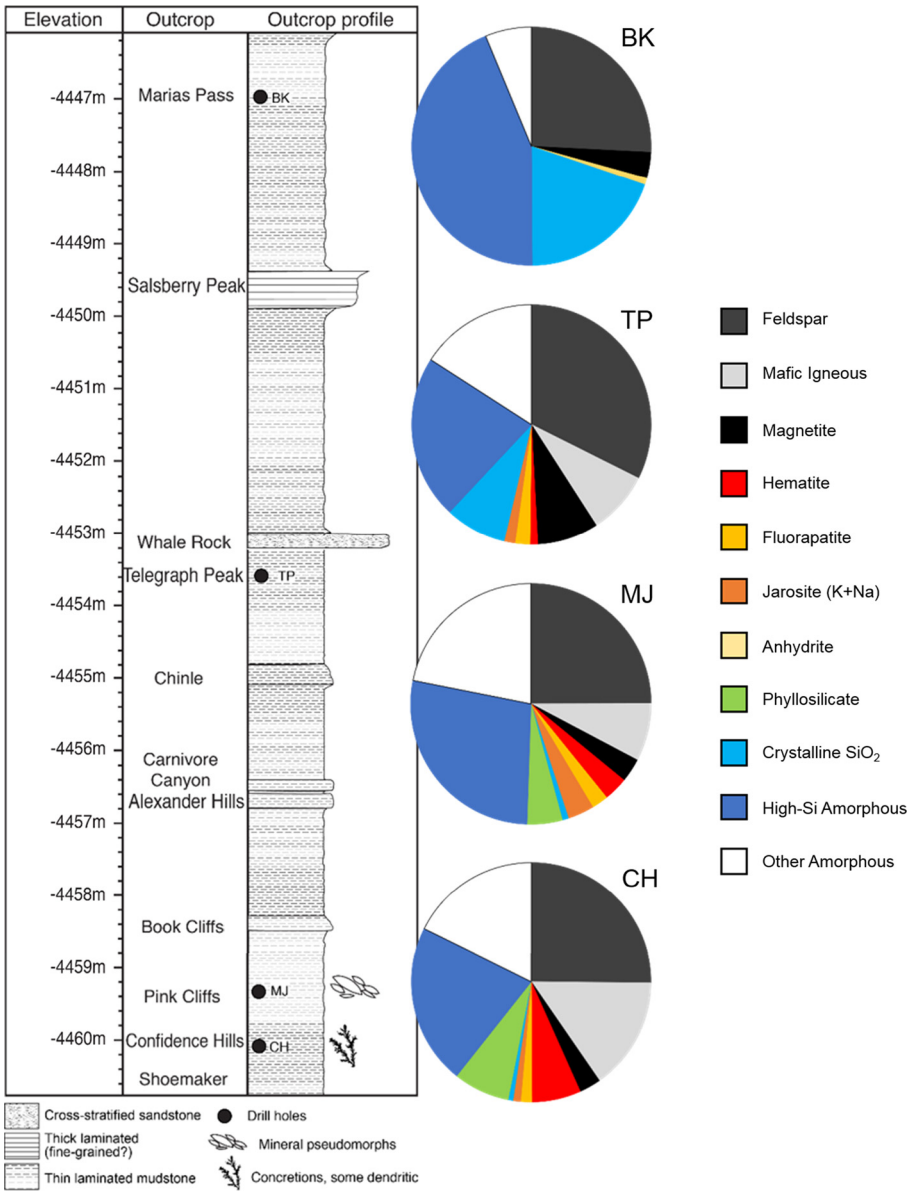

Fig. 4. Relative mineral abundances from CheMin in context with stratigraphy. "Feldspar" group includes plagioclase and sanidine. "Crystalline SiO_2" group includes quartz, cristobalite, and tridymite. "High-Si Amorphous" group includes rhyolitic glass, opal-A, and opal-CT. "Other amorphous" group includes basaltic glass and ferrihydrite.

depositional or diagenetic nature of minerals, the observed mineralogical and geochemical data in concert with the sedimentological observations provide evidence of stratigraphic trends within the Murray formation that can help elucidate the depositional and diagenetic history of this ancient lacustrine succession. There are distinct mineralogical differences between the samples measured at the base of the Pahrump Hills section and those measured progressively higher in the Murray formation, particularly with respect to the abundance and speciation of iron oxide minerals, mafic igneous minerals, and secondary silicate minerals (Fig. 4). Up section from the base of the Pahrump Hills section to Marias Pass, the abundance of mafic minerals diminishes, phyllosilicates give way to crystalline and amorphous SiO_2 phases, and the ratio of magnetite to hematite increases. The CH and MJ targets contain substantial abundances of mafic minerals (i.e., pyroxene), phyllosilicate minerals, and iron oxide minerals, as well as the greatest jarosite abundances. Hematite is the most abundant iron oxide in CH, whereas hematite and magnetite are present in equal abundances in MJ. Stratigraphically higher, in TP, the abundances of mafic minerals and jarosite decrease, there are no phyllosilicate minerals recorded, and magnetite is the dominant iron oxide. Crystalline SiO_2 (cristobalite) and opal-CT are abundant. Another 6 m up section, the BK sample from Marias Pass contains no mafic igneous minerals, phyllosilicate minerals, or jarosite; has less iron oxide than stratigraphically lower portions of the section (magnetite is the only crystalline iron oxide); yet has abundant crystalline SiO_2 (tridymite and minor cristobalite) and amorphous SiO_2.

In addition to mineralogical variation with stratigraphy, there are also trends in some minor and trace element abundances, as measured by APXS. At the base of the Pahrump Hills section, Zn and Ni are enriched up to 7.7 and 3.7 times that of average Mars crust (Taylor and McLennan, 2009), respectively (Fig. 5A), excluding Ni-enriched diagenetic features. Higher in the section, Zn and Ni abundances diminish and are depleted with respect to average Mars crust by over an order of magnitude in some targets in Marias Pass. Manganese shows a trend similar to those of Zn and Ni with stratigraphic position; however, Mn abundances are

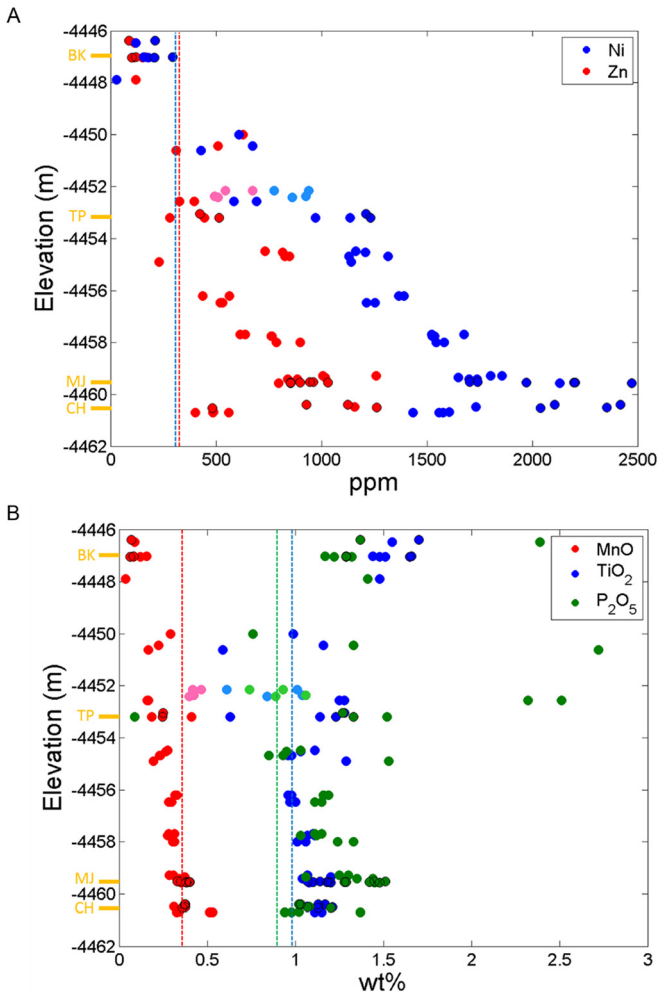

Fig. 5. Trace element abundances from APXS within the Murray formation with elevation: (A) Ni (in blue) and Zn (in red), where the vertical blue line represents average Mars crust composition of Ni (337 ppm); all averages from Taylor and McLennan (2009) and the vertical red line represents average Mars crust composition of Zn (320 ppm); and (B) MnO (in red), TiO_2 (in blue), and P_2O_5 (in green), where the vertical red line represents average Mars crust composition of MnO (0.36 wt.%), the vertical blue line represents average Mars crust composition of TiO_2 (0.98 wt.%), and the vertical green line represents average Mars crust composition of P_2O_5 (0.9 wt.%). Measurements from Whale Rock are in pink, light blue, and light green. Points outlined in black represents measurements on dust-removed surfaces. Elevations of drilled samples CH, MJ, TP, and BK samples are denoted n the y-axis in yellow.

close to those of average Mars crust at the base of the Pahrump Hills, rather than being enriched, and Mn becomes increasingly depleted upward in the section (Fig. 5B). Trends in Zn and Ni continue within and across the interbedded cross-laminated sandstone at Whale Rock interpreted as fluvial-deltaic facies prograding into a lake (Fig. 5A, Grotzinger et al., 2015). The continuation of the trace element trends through Whale Rock may suggest that the process which caused these trends influenced both mudstone and sandstone facies. Titanium abundances below Whale Rock do not show a distinct trend and they are close to, or slightly elevated above those of average Mars crust (Fig. 5B). Titanium, however, is enriched 1.7 times relative to average Mars crust in Marias Pass (Taylor and McLennan, 2009). Phosphorus behaves similarly to TiO_2 in the section and is enriched relative to average Mars crust by a comparable factor in Marias Pass (Fig. 5B). The significance of these enrichments is described below.

4.2. Models for depositional and diagenetic processes in the Murray formation

The sedimentary rocks of the Murray formation record mineralogical and geochemical variations that indicate a complex aqueous history. The *Curiosity* science team has developed multiple working hypotheses to explain these variations, including changing redox conditions in a neutral-alkaline lake (Hurowitz et al., in press). Based on terrestrial observations in acid-sulfate soils, acidic evaporite lakes, and basinal brines, we propose models involving deposition and/or diagenesis under variable pH solutions with potentially variable redox conditions to explain the observed mineralogy and geochemistry.

The Murray formation is dominantly composed of finely laminated mudstone with sub-horizontal laminae that extend laterally over distances of several meters (Grotzinger et al., 2015). As such, conceptual models to explain the mineralogy and chemistry of the mudstone involve sediment deposition in a subaqueous, lacustrine environment (Fig. 6). The absence of physical sedimentary evidence for subaerial exposure in the lacustrine succession suggests a perennial lake environment (Grotzinger et al., 2015). The heterogeneity of igneous minerals detected by CheMin through the section suggests that the source of the Murray sediments is itself heterogeneous or that deposition represents multiple sediment sources of different compositions (Siebach, 2016). Tridymite, sanidine, plagioclase, and high-silica glass are found together in silicic volcanic deposits on Earth (e.g., Broxton et al., 1995), and their discovery in BK is evidence for a possible silicic volcanic source (Morris et al., 2016). The abundance of pyroxene and the absence of crystalline SiO_2 at the base of the Pahrump Hills section suggest a potentially more primitive magma source for the detrital minerals.

4.2.1. Diagenesis in acidic groundwater

In our preferred hypothesis, we propose that the entirety of the lacustrine sequence was deposited in dilute lake waters with near-neutral pH and low Eh, and magnetite was deposited throughout the entirety of the section. Magnetite is unstable in long-lived, acidic and oxidizing conditions and readily transforms to maghemite and hematite (e.g., Schwertmann and Cornell, 2000; Otake et al., 2007). Thus, we hypothesize that the mudstone records deposition in near-neutral (e.g., buffered by basalt), low Eh lake waters (Fig. 6C) that prevented the oxidation of magnetite (magnetite is stable in waters on the Earth's surface with pH >8, Eh < -0.3; Drever, 1997). The magnetite could be either detrital or authigenic. The high abundance of magnetite in TP indicates that, if magnetite was detrital, the source region was enriched in magnetite or that physical sorting processes concentrated the mineral.

After sediment deposition, we hypothesize that multiple influxes of acidic groundwater moved through the sediments to dissolve detrital minerals, precipitate secondary phases, and mobilize certain trace and minor elements to produce the observed trends (Figs. 6E and 7). Oxic, and at least locally acidic, brines could have selectively affected the base of the Pahrump Hills, where the phyllosilicates acted as an aquitard, and caused the transformation of magnetite to hematite. These brines could have oxidized existing Fe-sulfide minerals to form jarosite or, if H_2SO_4 was present in solution, Fe that was leached and oxidized from the dissolution of magnetite could have combined with aqueous SO_4^{2-} to precipitate jarosite. Mixing of groundwater brines with different salinities could have caused the precipitation of gypsum in the sediment (e.g., Raup, 1982), which we infer from the lenticular crystal molds observed in MJ. A later diagenetic event then would have overprinted the trace element trends with elevation onto the mineralogy.

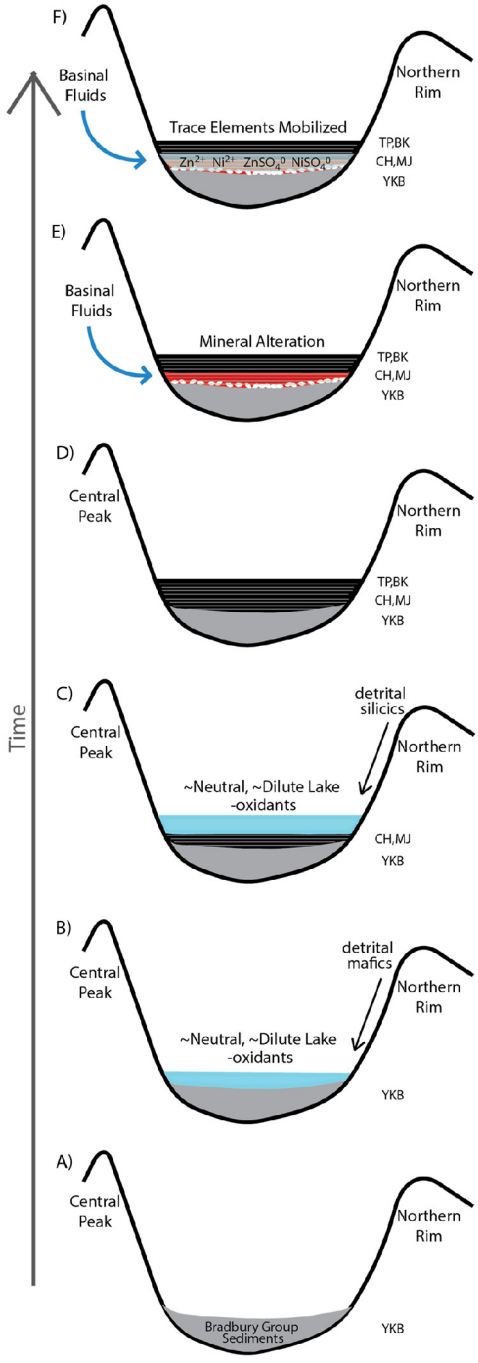

Fig. 6. Conceptual model of deposition and diagenesis of the Murray formation. A) Fluvial, lacustrine, and eolian sediments of the Bradbury group (including the lacustrine sediments at Yellowknife Bay, YKB) were deposited before and coevally with the Murray formation. B) Sediments at the base of the Pahrump Hills (represented by CH and MJ samples) were deposited in a lake with near-neutral, dilute waters with few oxidants. The detrital sediments had a primitive, mafic source. C) Later stages of the lake (represented by TP and BK samples) also had neutral and dilute lake waters without substantial oxidants, but detrital sediments included more evolved, silicic sources than the sediments at the base of the Pahrump Hills. Finely laminated lacustrine sediments of the lower Murray formation contained magnetite throughout (D) and experienced early diagenesis from multiple episodes of groundwaters to cause dissolution of detrital minerals and precipitation of new minerals (e.g., oxidation of magnetite to form hematite, precipitation of jarosite, and precipitation of gypsum) (E) and mobilize elements (F). Pore fluids were mildly acidic and oxic, mobilizing trace elements (e.g., Zn and Ni, primarily as Zn^{2+}, $ZnSO_4^0$, Ni^{2+}, and $NiSO_4^0$) and major elements, where they precipitated as sulfate salts (e.g., Mg–Ni-sulfate concretions) and/or chemisorbed to the surfaces of iron oxides and phyllosilicates, particularly at the base of the Pahrump Hills outcrop (F). Here, phyllosilicates may have acted as an aquitard.

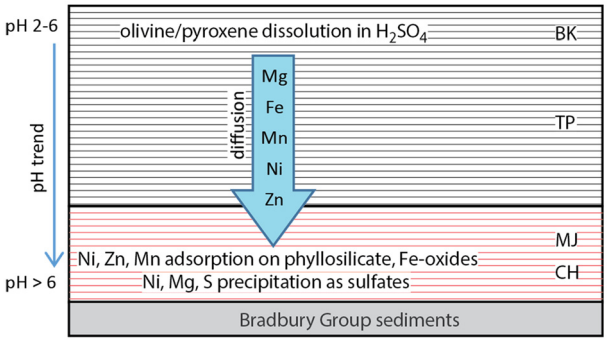

Fig. 7. Conceptual model of diagenetic event that created elemental trends within the stratigraphy. Briney pore fluids containing H_2SO_4 moved from the top of the section down. Mildly to moderately acidic brines preferentially leached mafic minerals to release Mg^{2+}, Fe^{2+}, Mn^{2+}, Ni^{2+}, and Zn^{2+} in solution. Brines could not have been extremely acidic because they would have mobilized Ti. As the brines moved down section and dissolved mafic minerals, the pH would have gradually risen. When brines encountered hematite and phyllosilicates in the lower Murray, Ni^{2+}, Zn^{2+}, and Mn^{2+} would have adsorbed onto mineral surfaces (particularly if the pH was >6) and precipitated as discrete mineral phases. Ni, Mg, and S would have also precipitated as sulfates, as observed in diagenetic features measured by APXS (e.g., VanBommel et al., 2016).

The mobility of Zn, Ni, and Mn in fluid-rich environments on Earth is controlled by the elements' pH-dependent aqueous speciation, saturation with respect to mineral phases, and the adsorptive capacity of available mineral surfaces (e.g., McBride, 1989; Stoffell et al., 2008; Degryse et al., 2009). Of all of these factors, pH is the most important determinant of the mobility of Zn, Ni, and Mn (Kiekens, 1995; McGrath, 1995; Degryse et al., 2009), where low pH can more effectively leach these trace elements from mafic mineral hosts. In general, enrichment of trace metals in terrestrial sedimentary basins occurs when trace elements are concentrated in moderately acidic to near-neutral, anoxic basinal brines (e.g., Kharaka et al., 1987; Stoffell et al., 2008), and Zn, in particular, is one of the most soluble and mobile of the trace metals in moderately acidic (pH <6), oxic surface waters (e.g., Rampe and Runnells, 1989; McBride, 1994; Drever, 1997). Changes in environmental conditions cause the precipitation of Zn, Ni, and Mn as discrete oxides (e.g., zincite, bunsenite, birnessite), oxyhydroxides (sweetite, theophrastite, pyrochroite), sulfides (sphalerite, millerite, rambergite), and sulfates (goslarite, morenosite, jokokuite). Alternatively, Zn, Ni, and Mn can co-precipitate with and substitute for Fe within the structures of hematite, magnetite, and clay minerals (Alloway, 1995; Kiekens, 1995). Adsorption on available mineral surfaces can also affect the fate of trace elements in the natural environment. At pH > 6, Zn^{2+}, Ni^{2+}, and Mn^{2+} readily chemisorb onto hematite and phyllosilicate surfaces (McBride, 1994; Yu et al., 1997). In contrast to Zn and Ni, Mn is a redox sensitive element and its mobility is primarily controlled by redox potential of the solutions, where low Eh causes abiotic reduction of Mn oxides to soluble and mobile Mn^{2+}, for instance in the presence of aqueous Fe(II) (e.g., Postma and Appelo, 2000).

We hypothesize that late-stage, mildly acidic pore fluids moved through the Murray formation succession at Pahrump Hills and Marias Pass, mobilized Zn, Ni, and Mn (and major elements, such as Mg and Fe), and caused passive enrichment of TiO_2 in Marias Pass (Fig. 7). These fluids may have also had a low Eh to keep Mn mobile as Mn^{2+}. Zn, Ni, and Mn can substitute for Mg and Fe in ferromagnesian minerals (e.g., olivine, pyroxene), and we suspect dissolution of ferromagnesian minerals in diagenetic fluids caused the enrichment of Zn and Ni at the base of the Pahrump Hills. If we assume that waters were acidified by H_2SO_4, and these acidic fluids were denser than existing pore fluids (e.g., contained more dissolved salts), then they would have moved from Marias Pass down toward the base of the Pahrump Hills to dissolve ferromag-

nesian minerals, mobilize trace and major elements, and create the depletions seen in Marias Pass. As a result, released Zn and Ni would primarily travel downslope as Zn^{2+}, $ZnSO_4^0$, Ni^{2+}, and $NiSO_4^0$ species in solution, and equilibrium modeling demonstrates that the pH of these fluids would have been <6 to keep Zn and Ni in solution (Figure S3). As these fluids traveled down through the sediments, they interacted with mafic minerals, which caused the solution pH to rise. At the base of the Pahrump Hills, the fluids encountered mineral surfaces (i.e., phyllosilicate and hematite) onto which trace element cations could chemisorb at pH >6, and the phyllosilicates may have acted as an aquitard to allow pore fluids to collect and concentrate. The correlation of Ni, Mg, and S in the cm-scale diagenetic crystal clusters suggests the mobilized species (e.g., $NiSO_4^0$) also precipitated as sulfate salts (VanBommel et al., 2016). These diagenetic fluids were likely short-lived because many minerals remain that would have been out of equilibrium with respect to the diagenetic fluids (e.g., feldspars, magnetite, jarosite, and olivine, where olivine dissolves readily at low pH (e.g., Wogelius and Walther, 1991) and has an expected lifetime of ~10 yr in basalt exposed to a water-limited acidic environment, based on laboratory dissolution rates; Hurowitz and McLennan, 2007), and we do not see evidence for secondary minerals that are indicative of extreme acid leaching environments (e.g., Al-clay minerals, Al-oxyhydroxides, goethite). Furthermore, these diagenetic fluids need not be extremely acidic because Zn, Ni, and Mn are highly mobile even under moderate acidity (pH ~4–6; McBride, 1994). The mobility of trace elements over meters of section suggests that diagenesis occurred in an open hydrologic system.

Titanium enrichment in Marias Pass may indicate passive enrichment from immobility. Titanium is highly mobile in solutions with extreme pH (i.e., pH < 2, pH > 12), in hydrothermal or metamorphic environments, and during advanced laterization (Van Baalen, 1993; Du et al., 2012; Bowen et al., 2013). Titanium, however, is immobile in nearly all terrestrial aqueous environments, including weathering profiles (e.g., Eggleton et al., 1987). In most aqueous environments, Ti in high-temperature minerals (ilmenite, titanomagnetite, titanite, perovskite) is released as they dissolve and immediately precipitated as secondary ilmenite, rutile, or anatase (Tilley and Eggleton, 2005; Du et al., 2012); thus, Ti can be mobile on the scale of mineral grains, but not on the scale of outcrops (Tilley and Eggleton, 2005). Titanium enrichment might imply that extreme pH conditions never occurred in Marias Pass.

The indication of cation-deficient magnetite in all samples may further support our proposed model of diagenesis in acidic groundwater. Magnetite in all samples from the Murray formation has a small unit cell (~8.35–8.36 Å) relative to stoichiometric magnetite (8.396 Å; e.g., Murad and Cashion, 2004). The small unit-cell lengths can represent vacancies in the structure, a substitution like $3\ Fe^{2+} = 2\ Fe^{3+} + \square$ that yields cation-deficient magnetite. Formation of cation-deficient magnetite can occur by heating magnetite to 250° C in an oxic environment (Schwertmann and Cornell, 2000) or by leaching Fe^{2+} from the structure with acidic solutions (pH 2–2.5; Jolivet and Tronc, 1988). We do not observe low-grade metamorphic phases in Gale crater and, as such, we interpret the small magnetite unit-cell as a product of the diagenetic fluids that created the observed trace element trends. Alternatively, cation-deficient magnetite may have precipitated from the lake waters (e.g., Tosca and Hurowitz, 2014; Tosca et al., 2016).

4.2.2. Deposition in a lake with changing pH and redox conditions

An alternative explanation for the mineral trends throughout the section, particularly with respect to the iron oxide minerals, is that the redox potential of the lake waters changed over time, wherein the lower portion of the Pahrump Hills section records an environment of high Eh, and the upper portions of the Pahrump Hills section and Marias Pass reflect a low Eh (Hurowitz et al., in press). The mineral assemblages and certain diagenetic features may also point towards changing pH in the lake waters over time. In acidic lake systems of Western Australia, for instance, hematite, jarosite, and phyllosilicate minerals precipitate during evapoconcentration of acidic (pH < 4), oxidizing shallow lake waters and groundwater (Benison and Bowen, 2006; Baldridge et al., 2009; Bowen et al., 2012). Millimeter-scale lenticular crystals morphologically similar to gypsum are observed in the lower portions of Pahrump Hills and are consistent with those seen in modern acidic evaporite lake environments (Benison and Bowen, 2006; Baldridge et al., 2009). Gypsum crystals and a variety of diagenetic concretions form in shallow groundwater while preserving fine lamination (Benison and Bowen, 2006; Benison et al., 2007). The physical sedimentological observations in the Pahrump Hills and Marias Pass, however, do not provide evidence for desiccation and subaerial exposure in this interval, and there is an absence of textures associated with desiccation of muds (e.g., desiccation cracks, prism cracks, intraclasts, tepee structures, and halo turbation).

4.2.3. Unresolved observations

Some observations are not explained by our conceptual model of deposition and diagenesis. The persistence of magnetite is problematic, but could be rationalized if the acidic waters were not long-lived. The biggest disparity, however, is the detection of minor amounts of fluorapatite throughout the Pahrump Hills. Fluorapatite is highly susceptible to dissolution in acidic fluids (e.g., Chaïrat et al., 2007; Hurowitz and McLennan, 2007), and yet the sample with the most fluorapatite (MJ) also has the most jarosite (indicative of acid-sulfate solutions of pH < 4). This paradox can be explained in three ways: 1) detrital fluorapatite was attacked by acid-sulfate fluids, but the fluids were not present long enough to dissolve all fluorapatite; 2) fluorapatite dissolution was inhibited by the precipitation of iron phosphate minerals (e.g., Berger et al., 2016) or by the adsorption of Zn to fluorapatite surfaces (Chin and Nancollas, 1991); or 3) fluorapatite is a late-stage precipitate and formed as the acidic fluids neutralized or after the acidic solutions had passed through the sediments. Data from the ChemCam instrument provide geochemical evidence for this last process; detections of Ca and F, interpreted as fluorapatite and fluorite (Forni et al., 2016), are generally associated with post depositional light-toned sulfate veins in the lower part of the Pahrump outcrop (Nachon et al., 2017). Precipitation of fluorapatite and trace metals Zn, Ni, and Mn may have been concomitant, where neutralization of acidic, phosphate-bearing fluids by interactions with mafic minerals could have raised pH into the fluorapatite stability field.

In addition to the presence of fluorapatite in Pahrump Hills, we observe an enrichment in P_2O_5 and TiO_2 in Marias Pass (Fig. 5B). Enrichments in both P_2O_5 and TiO_2 are uncommon in terrestrial weathering environments, but have been observed in the Scotian Basin, off the coast of Nova Scotia, where Ti mobility in meteoric water may be enhanced in the presence of P from the formation of Ti–P complexes (Pe-Piper et al., 2011). Diagenetic TiO_2 minerals form concurrently with secondary phosphate minerals (fluorapatite and crandallite) in the Scotian Basin. TiO_2 and P_2O_5 correlate with FeO in the Scotian Basin, and it has been proposed that Ti is present in ilmenite, whereas P is chemisorbed onto Fe-oxide mineral surfaces (Gould et al., 2010). We do not observe a correlation between Ti, P, and Fe, so this is an unlikely scenario for the Murray formation. Associations between TiO_2 and P_2O_5 could be an igneous signature of the original sediment source (Siebach, 2016). On Earth, for example, high relative abundances of TiO_2 and P_2O_5 are observed in ocean island basalts (Mullen, 1983).

4.2.4. Potential sources of acidity

The detection of jarosite in samples from the Pahrump Hills indicates that there were acid-sulfate fluids present at times with a pH < 4 (e.g., Driscoll and Leinz, 2005). This acidity, however, was not extreme, and the Murray formation is not enriched in SO_3 compared to average Mars crust, creating a strong contrast, for example, with what has been documented at Meridiani Planum for the Burns formation (McLennan et al., 2005; Hurowitz and McLennan, 2007; Squyres and Knoll, 2005). There are multiple potential sources for this restricted acidity. We favor oxidation of Fe-sulfides and/or dissolution of Fe-sulfates in groundwater or interaction between magmatic volatiles and groundwater as mechanisms that created acidic diagenetic fluids. Oxidative weathering of sulfide minerals produces extreme acidity through the generation of H_2SO_4 as observed in acid sulfate soils and acid mine drainage on Earth (e.g., Carson et al., 1982; Evangelou and Zhang, 1995). Sulfides have been detected in the Sheepbed mudstone near the detection limit of the CheMin instrument (1 wt.% pyrrhotite; Vaniman et al., 2014).

Magmatic and volcanic gases are another potential source of acidic volatiles. Regional or global volcanic exhalations of SO_2 and H_2S could produce H_2SO_4 if H_2S was oxidized and combined with atmospheric H_2O (i.e., acid rain or acid fog; Fairén et al., 2004), if they were deposited as aerosols in glaciers and subsequently melted (Zolotov and Mironenko, 2007), or if SO_2 thermally or photochemically disproportionated to form SO_3 and S (e.g., Marvin and Reiss, 1978) and combined with H_2O (e.g., Akhmatskaya et al., 1997). Impacts could remobilize and oxidize SO_2 so that it combined with H_2O in cooling impact plumes and clouds and rained out as H_2SO_4 (Fairén et al., 2004; Zolotov and Mironenko, 2007). Degassed SO_2 and H_2S into an early reducing Mars atmosphere may have initially been deposited in sediments as sulfites, then transformed to sulfate in a later oxidizing environment to produce acidity (Halevy et al., 2007). However, the absence of extensive leaching of the Murray formation, along with minimal evidence for diagenesis in the Bradbury group (McLennan et al., 2014; Vaniman et al., 2014; Siebach, 2016; Treiman et al., 2016) suggests we have not yet observed these widespread effects in the Gale crater system.

If magma was present in the near subsurface, it could have degassed SO_2 and H_2S into Gale crater's groundwater system, making the water acidic (e.g., Szynkiewicz et al., 2012). Impacts, such as the one that created Gale crater, can create new magma bodies from the unloading and partial melting of underlying mantle (Edwards et al., 2009) and can create deep fracture networks along which magma can travel (Schultz and Glicken, 1979). A similar process may be responsible for massive alunite deposits in Cross crater (Ehlmann et al., 2016). However, evidence for post-impact igneous activity in Gale crater is limited (Sautter et al., 2015) and basin temperatures are relatively low (Borlina et al., 2015).

After the formation of Fe-sulfates from acidic fluids, their dissolution and remobilization in groundwater would make the groundwater acidic. Jarosite dissolves incongruently in solutions with pH > 4 to produce acidity by the following reaction (Fairén et al., 2004; Welch et al., 2008):

$$KFe_3(SO_4)_2(OH)_6 + 3H_2O \rightarrow 3Fe(OH)_3 + K^+ + 3H^+ + 2SO_4^{2-}$$

Experimental dissolution of jarosite in a solution with a pH 8 (near the pH of water buffered by basalt) shows that this reaction can drive the pH to extreme acidity (pH ~3.3; Smith et al., 2006). Interaction between pore fluids and Fe-sulfate deposits could have caused acidic diagenesis in the Murray formation.

5. Conclusions

Lacustrine mudstone of the Murray formation is mineralogically diverse from the base of the section at Pahrump Hills through higher stratigraphic levels at Marias Pass. The Confidence Hills sample, at the base of the section, contains abundant plagioclase, pyroxene, phyllosilicate, hematite, and X-ray amorphous material with minor jarosite. Moving up section, abundances of pyroxene, hematite, and phyllosilicate decrease; magnetite becomes the prevalent iron oxide mineral; and crystalline SiO_2 phases (cristobalite and tridymite) become abundant. Jarosite is most abundant in the MJ sample, about 1 m stratigraphically up section from CH. In addition to these trends in mineral proportions, abundances of the trace elements Zn, Ni, and Mn gradually decrease up section. The laterally continuous, sub-horizontal, fine lamination and fine grain size observed throughout the mudstone in the Murray formation indicate sediment deposition from suspension in an ancient lake environment, which we suspect had dilute lake waters with near-neutral pH. We hypothesize that early diagenesis from multiple influxes of acidic groundwaters then dissolved some minerals (e.g., magnetite), precipitated new phases (e.g., hematite, jarosite), and produced trace elements trends in Zn, Ni, and Mn with elevation. Alternatively, the mineralogical variations in the stratigraphy may be explained by sediment deposition in lake waters that had variable pH and Eh, where CH and MJ may have been deposited in acid evaporite lakes and TP and BK may have been deposited in lakes with neutral and dilute lake waters.

Acknowledgements

The authors gratefully acknowledge support from the NASA Mars Science Laboratory Mission and the efforts of the MSL engineering and science operations teams. This manuscript was improved by thoughtful comments from Kathleen Benison and an anonymous reviewer.

Appendix A. Supplementary material

Supplementary material related to this article can be found online at http://dx.doi.org/10.1016/j.epsl.2017.04.021.

References

Akhmatskaya, E.V., Apps, C.J., Hillier, I.H., Masters, A.J., Watt, N.E., Whitehead, J.C., 1997. Formation of H_2SO_4 from SO_3 and H_2O, catalyzed in water clusters. Chem. Commun. 7, 707–708. http://dx.doi.org/10.1039/A700802C.

Alloway, B.J., 1995. Soil processes and the behavior of heavy metals. In: Alloway, B.J. (Ed.), Heavy Metals in Soils. Springer, pp. 11–37.

Anderson, R.C., Jandura, L., Okon, A.B., Sunshine, D., Roumeliotis, C., Beegle, L.W., Hurowitz, J., Kennedy, B., Limonadi, D., McCloskey, S., Robinson, M., Seybold, C., Brown, K., 2012. Collecting samples in Gale crater, Mars; an overview of the Mars Science Laboratory Sample Acquisition, Sample Processing and Handling system. Space Sci. Rev. 170, 57–75. http://dx.doi.org/10.1007/s11214-012-9898-9.

Baldridge, A.M., Hook, S.M., Crowley, J.K., Marion, G.M., Kargel, J.S., Michalski, J.R., Thomson, B.J., de Souza Filho, C.R., Bridges, N.T., Brown, A.J., 2009. Contemporaneous deposition of phyllosilicates and sulfates: using Australian acidic saline lake deposits to describe geochemical variability on Mars. Geophys. Res. Lett. 36. http://dx.doi.org/10.1029/2009GL040069.

Benison, K.C., Bowen, B.B., 2006. Acid saline lake systems give clues about past environments and the search for life on Mars. Icarus 183, 225–229. http://dx.doi.org/10.1016/j.icarus.2006.02.018.

Benison, K.C., Bowen, B.B., Oboh-Ikuenobe, F.E., Jagniecki, E.A., LaClair, D.A., Story, S.L., Mormile, M.R., Hong, B.-Y., 2007. Sedimentology of acid saline lakes in southern Western Australia: newly described processes and products of an extreme environment. J. Sediment. Res. 77, 366–388. http://dx.doi.org/10.2110/jsr.2007.038.

Berger, J.A., Schmidt, M.E., Izawa, M.R.M., Gellert, R., Ming, D.W., Rampe, E.B., VanBommel, S.J., McAdam, A.C., 2016. Phosphate stability in diagenetic fluids constrains the acidic alteration model for lower Mt. Sharp sedimentary rocks in Gale crater, Mars. In: LPS XLVII, 1652.

Blake, D.F., et al., 2012. Characterization and calibration of the CheMin mineralogical instrument on Mars Science Laboratory. Space Sci. Rev. 170, 341–399. http://dx.doi.org/10.1007/s11214-012-9905-1.

Borlina, C.S., Ehlmann, B.L., Kite, E.S., 2015. Modeling the thermal and physical evolution of Mount Sharp's sedimentary rocks, Gale Crater, Mars: implications for diagenesis on the MSL Curiosity rover traverse. J. Geophys. Res. 120, 1396–1414. http://dx.doi.org/10.1002/2015JE004799.

Bowen, B.B., Benison, K.C., Story, S., 2012. Early diagenesis by modern acid brines in Western Australia and implications for the history of sedimentary modification on Mars. Mars Sedimentology. SEPM Spec. Publ. 102, 229–252.

Bowen, B.B., Story, S., Oboh-Ikuenobe, F., Benison, K.C., 2013. Differences in regolith weathering history at an acid and neutral saline lake on the Archean Yilgarn Craton and implications for acid brine evolution. Chem. Geol. 356, 126–140. http://dx.doi.org/10.1016/j.chemgeo.2013.08.005.

Bristow, T.F., et al., 2015. The origin and implications of clay minerals from Yellowknife Bay, Gale crater, Mars. Am. Mineral. 100, 824–836. http://dx.doi.org/10.2138/am-2015-5077CCBYNCND.

Broxton, D.E., Heiken, G.H., Chipera, S., Byers Jr., F.M., 1995. Stratigraphy, petrography, and mineralogy of Bandalier Tuff and Cerro Toledo deposits. In: Broxton, D.E., Eller, G.G. (Eds.), Earth Science Investigations for Environmental Restoration – Los Alamos National Laboratory, Technical Area 21. In: Los Alamos National Lab. Rep.. LA-12934-MS, 118 pp.

Campbell, J.L., Perrett, G.M., Gellert, R., Andrushenko, S.M., Boyd, N.I., Maxwell, J.A., King, P.L., Schofield, C.D.M., 2012. Calibration of the Mars Science Laboratory Alpha Particle X-ray Spectrometer. Space Sci. Rev. 170, 319–340. http://dx.doi.org/10.1007/s11214-012-9873-5.

Carson, C., Fanning, D., Dixon, J., 1982. Alfisols and Ultisols with acid sulfate weathering features in Texas. In: Kittrick, J., Fanning, D., Hossner, K. (Eds.), Acid Sulfate Weathering. In: SSSA Spec. Publ., vol. 10. SSSA, Madison, WI, pp. 127–146.

Chaïrat, C., Schott, J., Oelkers, E.H., Lartigue, J.-E., Harouiya, N., 2007. Kinetics and mechanism of natural fluorapatite dissolution at 25 °C and pH from 3 to 12. Geochim. Cosmochim. Acta 71, 5901–5912. http://dx.doi.org/10.1016/j.gca.2007.08.031.

Chin, K.O.A., Nancollas, G.H., 1991. Dissolution of fluorapatite. A constant-composition kinetics study. Langmuir 7, 2175–2179. http://dx.doi.org/10.1021/la00058a034.

Chipera, S.J., Bish, D.L., 2002. FULLPAT: a full pattern quantitative analysis program for X-ray powder diffraction using measured and calculated patterns. J. Appl. Crystallogr. 35, 744–749. http://dx.doi.org/10.1107/S0021889802017405.

Collyer, S., 1986. Crystallographic Studies of Magnetite and Titanomaghemite. Ph.D. thesis. University of Aston in Birmingham.

Degryse, F., Smolders, E., Parker, D.R., 2009. Partitioning of metals (Cd, Co, Cu, Ni, Pb, Zn) in soils: concepts, methodologies, prediction and applications – a review. Eur. J. Soil Sci. 60, 590–612. http://dx.doi.org/10.1111/j.1365-2389.2009.01142.x.

Drever, J.I., 1997. The Geochemistry of Natural Waters: Surface and Groundwater Environments, third ed. Prentice Hall. 436 p.

Driscoll, R.L., Leinz, R.W., 2005. Methods for synthesis of some jarosites. USGS Tech. Methods 5-D1. 5 pp.

Du, X., Rate, A.W., Gee, M.A.M., 2012. Redistribution and mobilization of titanium, zirconium and thorium in an intensely weathered lateritic profile in Western Australia. Chem. Geol. 330–331, 101–115. http://dx.doi.org/10.1016/j.chemgeo.2012.08.030.

Edwards, C.S., Bandfield, J.L., Christensen, P.R., Fergason, R.L., 2009. Global distribution of bedrock exposures on Mars using THEMIS high-resolution thermal inertia. J. Geophys. Res., Planets 114. http://dx.doi.org/10.1029/2009JE003363.

Eggleton, R.A., Foudoulis, C., Varkevisser, D., 1987. Weathering of basalt: changes in rock chemistry and mineralogy. Clays Clay Miner. 35, 161–169. http://dx.doi.org/10.1346/CCMN.1987.0350301.

Ehlmann, B.L., Swayze, G.A., Milliken, R.E., Mustard, J.F., Clark, R.N., Murchie, S.L., Breit, G.N., Wray, J.J., Gondet, B., Poulet, F., Carter, J., Calvin, W.M., Benzel, W.M., Seelos, K.D., 2016. Discovery of alunite in Cross crater, Terra Sirenum, Mars: evidence for acidic, sulfurous waters. Am. Mineral. 101. http://dx.doi.org/10.2138/am-2016-5574.

Evangelou, V.P., Zhang, Y.L., 1995. A review: pyrite oxidation mechanisms and acid mine drainage prevention. Crit. Rev. Environ. Sci. Technol. 25. http://dx.doi.org/10.1080/10643389509388477.

Fairén, A.G., Fernández-Remolar, D., Dohm, J.M., Baker, V.R., Amils, R., 2004. Inhibition of carbonate synthesis in acidic oceans on early Mars. Nature 431, 423–426.

Forni, O., et al., 2016. Fluorine in the Pahrump outcrop, Gale crater: implications for fluid circulation and alteration. In: LPS XLVII, 1990.

Fraeman, A.A., Arvidson, R.E., Catalano, J.G., Grotzinger, J.P., Morris, R.V., Murchie, S.L., Stack, K.M., Humm, D.C., McGovern, J.A., Seelos, F.P., Seelos, K.D., Viviano, C.E., 2013. A hematite-bearing layer in Gale Crater, Mars: mapping and implications for past aqueous conditions. Geology 41, 1103–1106. http://dx.doi.org/10.1130/G34613.1.

Gellert, R., Berger, J.A., Boyd, N., Campbell, J.L., Desouza, E.D., Elliot, B., Fisk, M., Pavri, B., Perrett, G.M., Schmidt, M., Thompson, L., VanBommel, S., Yen, A.S., 2015a. Chemical evidence for an aqueous history at Pahrump, Gale crater, Mars, as seen by the APXS. In: LPS XLVI, 1855.

Gellert, R., Clark, B.C., MSL and MER Science Teams, 2015b. In-situ compositional measurements of rocks and soils with the Alpha Particle X-ray Spectrometer on NASA's Mars rovers. Elements 11, 39–44. http://dx.doi.org/10.2113/gselements.11.1.39.

Gould, K., Pe-Piper, G., Piper, D.J.W., 2010. Relationship of diagenetic chlorite rims to depositional facies in Lower Cretaceous reservoir sandstones of the Scotian Basin. Sedimentology 57, 587–610. http://dx.doi.org/10.1111/j.1365-3091.2009.01106.x.

Grotzinger, J.P., et al., 2012. Mars Science Laboratory mission and science investigation. Space Sci. Rev. 170, 5–56. http://dx.doi.org/10.1007/s11214-012-9892-2.

Grotzinger, J.P., et al., 2014. A habitable fluvio-lacustrine environment at Yellowknife Bay, Gale crater, Mars. Science 343, 6169. http://dx.doi.org/10.1126/science.1242777.

Grotzinger, J.P., et al., 2015. Deposition, exhumation, and paleoclimate of an ancient lake deposit, Gale crater, Mars. Science 350, 6257. http://dx.doi.org/10.1126/science.aac7575.

Halevy, I., Zuber, M.T., Schrag, D.P., 2007. A sulfur dioxide climate feedback on early Mars. Science 318, 1903–1907. http://dx.doi.org/10.1126/science.1147039.

Hurowitz, J.A., McLennan, S.M., 2007. A ∼3.5 Ga record of water-limited, acidic weathering conditions on Mars. Earth Planet. Sci. Lett. 260, 432–443. http://dx.doi.org/10.1016/j.epsl.2007.05.043.

Hurowitz, J.A. et al., in press. Redox stratification of an ancient lake in Gale Crater, Mars. Science. http://dx.doi.org/10.1126/science.aah6849.

Jolivet, J.-P., Tronc, E., 1988. Interfacial electron transfer in colloidal spinel iron oxide. Conversion of Fe_3O_4–γFe_2O_3 in aqueous medium. J. Colloid Interf. Sci. 125, 688–701. http://dx.doi.org/10.1016/0021-9797(88)90036-7.

Kah, L.C., Kronyak, R., Van Beek, J., Nachon, M., Mangold, N., Thompson, L., Wiens, R., Grotzinger, J., Farmer, J., Minitti, M., Schieber, J., Oehler, D., 2015a. Diagenetic crystal clusters and dendrites, lower Mount Sharp, Gale crater. In: LPS XLVI, 1901.

Kah, L.C., Kronyak, R.E., Van Beek, J., Nachon, M., Mangold, N., Thompson, L.M., Wiens, R.C., Grotzinger, J.P., Schieber, J., 2015b. Late diagenetic cements in the Murray formation, Gale crater, Mars: implications for postdepositional fluid flow. Abstract P53F-05 presented at 2015 Fall Meeting, AGU, San Francisco, Calif. 14–18 December.

Kharaka, Y.K., Maest, A.S., Carothers, W.W., Law, L.M., Lamothe, P.J., Fries, T.L., 1987. Geochemistry of metal-rich brines from central Mississippi Salt Dome basin, U.S.A. Appl. Geochem. 2, 543–561. http://dx.doi.org/10.1026/0883-2927(87)90008-4.

Kiekens, L., 1995. Zinc. In: Alloway, B.J. (Ed.), Heavy Metals in Soils. Springer, pp. 284–305.

Marvin, D.C., Reiss, H., 1978. Cloud chamber study of the gas photooxidation of sulfur dioxide. J. Chem. Phys. 69, 1897–1918. http://dx.doi.org/10.1063/1.436827.

McBride, M.B., 1989. Reactions controlling heavy metal solubility in soils. In: Advances in Soil Science. Springer, New York, pp. 1–56.

McBride, M.B., 1994. Environmental Chemistry of Soils. Oxford University Press, Inc., New York, NY.

McGrath, S.P., 1995. Chromium and nickel. In: Alloway, B.J. (Ed.), Heavy Metals in Soils. Springer, pp. 152–178.

McLennan, S.M., Bell III, J.F., Calvin, W.M., Christensen, P.R., Clark, B.C., de Sauza, P.A., Farmer, J., Farrand, W.H., Fike, D.A., Gellert, R., Ghosh, A., Glotch, T.D., Grotzinger, J.P., Hahn, B., Herkenhoff, K.E., Hurowitz, J.A., Johnson, J.R., Johnson, S.S., Joliff, B., Klingelhöfer, G., Knoll, A.H., Learner, Z., Malin, M.C., McSween Jr., H.Y., Pocock, J., Ruff, S.W., Soderblom, L.A., Squyres, S.W., Tosca, N.J., Watters, W.A., Wyatt, M.B., Yen, A., 2005. Provenance and diagenesis of the evaporite-bearing Burns formation, Meridiani Planum, Mars. Earth Planet. Sci. Lett. 240, 95–121.

McLennan, S.M., et al., 2014. Elemental geochemistry of sedimentary rocks at Yellowknife Bay, Gale crater, Mars. Science 343, 6169. http://dx.doi.org/10.1126/science.1244734.

Milliken, R.E., Grotzinger, P.P., Thomson, B.J., 2010. Paleoclimate of Mars as captured by the stratigraphic record in Gale Crater. Geophys. Res. Lett. 37, L16202. http://dx.doi.org/10.1029/2009GL041870.

Ming, D.W., et al., 2014. Volatile and organic compositions of sedimentary rocks in Yellowknife Bay, Gale crater, Mars. Science 343. http://dx.doi.org/10.1126/science.1245267.

Moore, D.M., Reynolds Jr., R.C., 1997. X-Ray Diffraction and the Identification and Analysis of Clay Minerals, 2nd ed. Oxford University Press, 378 pp.

Morris, R.V., et al., 2016. Silicic volcanism on Mars evidenced by tridymite detection in High-SiO_2 sedimentary rock at Gale crater. Proc. Natl. Acad. Sci. USA.

Mullen, E.D., 1983. $MnO/TiO_2/P_2O_5$: a minor element discriminant for basaltic rocks of oceanic environments and its implications for petrogenesis. Earth Planet. Sci. Lett. 62, 53–62. http://dx.doi.org/10.1016/0012-821X(83)90070-5.

Murad, E., Cashion, J., 2004. Mossbauer Spectroscopy of Environmental Materials and Their Industrial Utilization. Springer, p. 417.

Nachon, M., et al., 2017. Chemistry of diagenetic features analyzed by ChemCam at Pahrump Hills, Gale crater, Mars. Icarus 281, 121–136. http://dx.doi.org/10.1016/j.icarus.2016.08.026.

Otake, T., Wesolowski, D.J., Anovitz, L.M., Allard, L.F., Ohmoto, H., 2007. Experimental evidence for non-redox transformations between magnetite and hematite under H_2-rich hydrothermal conditions. Earth Planet. Sci. Lett. 257, 60–70. http://dx.doi.org/10.1016/j.epsl.2007.02.022.

Pe-Piper, G., Karim, A., Piper, D.J.W., 2011. Authigenesis of titania minerals and the mobility of Ti: new evidence from pro-deltaic sandstones, Cretaceous Scotian Basin, Canada. J. Sediment. Res. 81, 762–773. http://dx.doi.org/10.2110/jsr.2011.63.

Postma, D., Appelo, C.A.J., 2000. Reduction of Mn-oxides by ferrous iron in a flow system: column experiment and reactive transport modeling. Geochim. Cosmochim. Acta 64, 1237–1247. http://dx.doi.org/10.1016/S0016-7037(99)00356-7.

Rampe, J.J., Runnells, D.D., 1989. Contamination of water and sediment in a desert stream by metals from an abandoned gold mine and mill, Eureka District, Arizona. Appl. Geochem. 4, 445–454. http://dx.doi.org/10.1016/0883-2927(89)90002-4.

Raup, O.B., 1982. Gypsum precipitation by mixing seawater brines. Am. Assoc. Pet. Geol. Bull. 66, 363–367.

Sautter, V., et al., 2015. In situ evidence for continental crust on early Mars. Nat. Geosci. 8, 605–609. http://dx.doi.org/10.1038/NGEO2474.

Schultz, P.H., Glicken, H., 1979. Impact crater and basin control of igneous processes on Mars. J. Geophys. Res. 84, 8033–8047. http://dx.doi.org/10.1029/JB084iB14p08033.

Schwertmann, U., Cornell, R.M., 2000. Iron Oxides in the Laboratory: Preparation and Characterization, 2nd ed. Wiley–VCH, p. 188.

Siebach, K.L., 2016. Formation and Diagenesis of Sedimentary Rocks in Gale Crater, Mars. Ph.D. thesis. California Institute of Technology, p. 177.

Squyres, S.W., Knoll, A.H., 2005. Sedimentary rocks at Meridiani Planum: origin, diagenesis, and implications for life on Mars. Earth Planet. Sci. Lett. 240, 1–10. http://dx.doi.org/10.1016/j.epsl.2005.09.038.

Smith, A.M.L., Hudson-Edwards, K.A., Dubbin, W.E., Wright, K., 2006. Dissolution of jarosite [$KFe_3(SO_4)_2(OH)_6$] at pH 2 and 8: insights from batch experiments and computational modelling. Geochim. Cosmochim. Acta 70, 608–621. http://dx.doi.org/10.1016/j.gca.2005.09.024.

Stoffell, B., Appold, M.S., Wilkinson, J.J., McClean, N.A., Jeffries, T.E., 2008. Geochemistry and evolution of Mississippi Valley-Type mineralizing brines from the Tri-State and northern Arkansas districts determined by LA-ICP-MS microanalysis of fluid inclusions. Econ. Geol. 103, 1411–1435. http://dx.doi.org/10.2113/gsecongeo.103.7.1411.

Stout, M.Z., Bayliss, P., 1980. Crystal structure of two ferrian ulvospinels from British Columbia. Can. Mineral. 18, 339–341.

Szynkiewicz, A., Johnson, A.P., Pratt, L.M., 2012. Sulfur species and biosignatures in Sulphur Springs, Valles Caldera, New Mexico – implications for Mars astrobiology. Earth Planet. Sci. Lett. 321–322, 1–13. http://dx.doi.org/10.1016/j.epsl.2011.12.015.

Taylor, S.R., McLennan, S.M., 2009. Planetary Crusts: Their Composition, Origin and Evolution, vol. 10. Cambridge University Press.

Tosca, N.J., Hurowitz, J.A., 2014. Magnetite authigenesis and the ancient martian atmosphere. Paper presented at the Goldschmidt Conference, Sacramento, CA.

Tosca, N.J., Guggenheim, S., Pufahl, P.K., 2016. An authigenic origin for Precambrian greenalite: implications for iron formation and the chemistry of ancient seawater. GSA Bull. 128, 511–530. http://dx.doi.org/10.1130/B31339.1.

Treiman, A.H., Morris, R.V., Agresti, D.G., Graff, T.G., Achilles, C.N., Rampe, E.B., Bristow, T.F., Ming, D.W., Blake, D.F., Vaniman, D.T., Bish, D.L., Chipera, S.J., Morrison, S.M., Downs, R.T., 2014. Ferrian saponite from the Santa Monica Mountains, California, (U.S.A., Earth): Characterization as an analog for clay minerals on Mars with application to Yellowknife Bay in Gale Crater. Am. Mineral. 99, 2234–2250. http://dx.doi.org/10.2138/am-2014-4763.

Treiman, A.H., et al., 2016. Mineralogy, provenance, and diagenesis of a potassic basaltic sandstone on Mars: CheMin X-ray diffraction of the Windjana sample (Kimberley area, Gale Crater). J. Geophys. Res., Planets 121, 75–106. http://dx.doi.org/10.1002/2015JE004932.

Tilley, D.B., Eggleton, R.A., 2005. Titanite low-temperature alteration and Ti mobility. Clays Clay Miner. 53, 100–107. http://dx.doi.org/10.1346/CCMN.2005.0530110.

Van Baalen, M.R., 1993. Titanium mobility in metamorphic systems: a review. Chem. Geol. 110, 233–249.

VanBommel, S.J., Gellert, R., Berger, J.A., Campbell, J.L., Thompson, L.M., Edgett, K.S., McBride, M.J., Minitti, M.E., Pradler, I., Boyd, N.I., 2016. Deconvolution of distinct lithology chemistry through oversampling with the Mars Science Laboratory Alpha Particle X-ray Spectrometer. X-Ray Spectrom. 45, 155–161. http://dx.doi.org/10.1002/xrs.2681.

Vaniman, D.T., et al., 2014. Mineralogy of a mudstone at Yellowknife Bay, Gale crater, Mars. Science 343, 6169. http://dx.doi.org/10.1126/science.1243480.

Vasavada, A.R., Grotzinger, J.P., Arvidson, R.E., Calef, F.J., Crisp, J.A., Gupta, S., Hurowitz, J., Mangold, N., Maurice, S., Schmidt, M.E., Wiens, R.C., Williams, R.M.E., Yingst, A.R., 2014. Overview of the Mars Science Laboratory mission: Bradbury landing to Yellowknife Bay and beyond. J. Geophys. Res. 119, 1134–1161. http://dx.doi.org/10.1002/2014JE004622.

Welch, S.A., Kirste, D., Christy, A.G., Beavis, F.R., Beavis, S.G., 2008. Jarosite dissolution II – reaction kinetics, stoichiometry and acid flux. Chem. Geol. 254, 73–86. http://dx.doi.org/10.1016/j.chemgeo.2008.06.010.

Wogelius, R.A., Walther, J.V., 1991. Olivine dissolution at 25 °C: effects of pH, CO_2, and organic acids. Geochim. Cosmochim. Acta 55, 943–954. http://dx.doi.org/10.1016/0016-7037(91)90153-V.

Yu, T.R., Sun, H.Y., Zhang, H., 1997. Specific adsorption of cations. In: Yu, T.R. (Ed.), Chemistry of Variable Charge Soils. Oxford, pp. 140–174.

Zolotov, M.Y., Mironenko, M.V., 2007. Timing of acid weathering on Mars: a kinetic-thermodynamic assessment. J. Geophys. Res., Planets 112. http://dx.doi.org/10.1029/2006JE002882.